

# Broad Range of Neural Dynamics From a Time-Varying FitzHugh–Nagumo Model and its Spiking Threshold Estimation

Rose T. Faghih\*, *Student Member, IEEE*, Ketan Savla, Munther A. Dahleh, *Fellow, IEEE*, and Emery N. Brown, *Fellow, IEEE*

**Abstract**—We study the use of the FitzHugh–Nagumo (FHN) model for capturing neural spiking. The FHN model is a widely used approximation of the Hodgkin–Huxley model that has significant limitations. In particular, it cannot produce the key spiking behavior of bursting. We illustrate that by allowing time-varying parameters for the FHN model, these limitations can be overcome while retaining its low-order complexity. This extension has applications in modeling neural spiking behaviors in the thalamus and the respiratory center. We demonstrate the use of the FHN model from an estimation perspective by presenting a novel parameter estimation method that exploits its multiple time-scale properties, and compare the performance of this method with the extended Kalman filter in several illustrative examples. We demonstrate that the dynamics of the spiking threshold can be recovered even in the absence of complete specifications for the system.

**Index Terms**—Algorithms, biological system modeling, biomedical signal processing, parameter estimation .

## I. INTRODUCTION

SINCE the seminal work of Hodgkin and Huxley [10], there has been a continued interest in the dynamical systems viewpoint of a neuron. Hodgkin–Huxley (HH), Hindmarsh–Rose (HR) [18], and FitzHugh–Nagumo (FHN) [8], [14] models are among the most successful dynamical models in computational neuroscience for capturing neural spiking behaviors. A detailed explanation of these and several other models can be found in [11]. The HH model consists of four differential equa-

tions with many coefficients. Although this model is capable of generating all of the neural spiking behaviors, it is highly nonlinear. On the other hand, the HR model, which consists of three highly coupled differential equations, can exhibit all the spiking modes obtained from the HH model without the biophysical details [11]. Finally, the FHN model consists of two differential equations, and is simpler than the HH and HR models, though it is unable to exhibit important spiking behaviors such as bursting. In fact, it has been noted [11] that without using a reset or adding noise, the FHN model cannot exhibit bursting. Our focus is on *low complexity* models that can exhibit most of the neural spiking activities that can be produced by well-known dynamical systems models (such as the HH model). Here, we use the term *complexity* to refer to the presence of redundancies in the model in addition to its capability of capturing neural spiking behaviors, and difficulty in parameter estimation. With this in mind, we propose an extension to the FHN model that has time-varying parameters, under the assumption that the time variations of these parameters are physiologically programmed within a neuron. We also highlight the utility of the FHN model from an estimation perspective. We present a novel parameter estimation method that exploits the multiple time-scale feature of the FHN model, and compare the performance of this method with extended Kalman filter (EKF) through illustrative examples.

In Section II, we propose an extension to the FHN model by using a time-varying spiking threshold, and show that using this method it is possible to obtain tonic bursting, mixed mode firing, neural spiking with nonincreasing frequency, and varying frequency neural spiking. These spiking behaviors, which are observed in the thalamus and the respiratory center, can be obtained with higher order models, but not with the original FHN model. In Section III, using the fast–slow dynamics of the FHN model, we propose an algorithm, which we refer to as the Fast-Slow Dynamics (FSD) Estimation Algorithm, for estimating the spiking threshold in the FHN model. We compare the performance of FSD and EKF for the fixed parameter case through illustrative examples. The examples demonstrate that the FSD method outperforms EKF when the sensor noise variance is large or when the sampling rate is low. Then, we extend FSD to the case when the spiking threshold is varying slowly and one has some knowledge of the structure of the variations (e.g., oscillatory, impulsive, etc.) of this threshold. For this case, FSD outperforms EKF when the sampling rate is low. In order to run the FSD algorithm, only the spiking data are used and the

Manuscript received July 20, 2011; revised October 19, 2011; accepted November 13, 2011. Date of publication December 16, 2011; date of current version February 17, 2012. This work was supported in part by National Institutes of Health under Grant DP1 OD003646 and by the National Science Foundation (NSF) under Grant 0836720. The work of R. T. Faghih was supported in part by the Massachusetts Institute of Technology Fellowship in Control and NSF Graduate Fellowship. This paper was presented in part at the proceedings of the IEEE Engineering in Medicine and Biology Society Conference [5] and R. T. Faghih's Master's Thesis [6]. *Asterisk indicates corresponding author.*

\*R. T. Faghih is with the Laboratory for Information and Decision Systems, Massachusetts Institute of Technology, MA 02139 USA (e-mail: rfaghih@mit.edu).

K. Savla and M. A. Dahleh are with the Laboratory for Information and Decision Systems, Massachusetts Institute of Technology, MA 02139 USA (e-mail: ksavla@mit.edu; dahleh@mit.edu).

E. N. Brown is with the Department of Brain and Cognitive Sciences, Harvard–Massachusetts Division of Health Sciences and Technology, Massachusetts Institute of Technology, Cambridge, MA 02139 USA, with the Harvard Medical School, Boston, MA 02115 USA, and also with the Department of Anesthesia, Critical Care and Pain Medicine, Massachusetts General Hospital, Boston, MA 02114 USA (e-mail: enbrown1@mit.edu).

Digital Object Identifier 10.1109/TBME.2011.2180020

spiking threshold is estimated without using the values of the parameters of the FHN model. However, in order to apply the EKF algorithm, in addition to using the spiking data, we also assumed that all of the parameters of the FHN model except for the spiking threshold are known.

## II. FHN MODEL WITH TIME-VARYING THRESHOLD

A simplified version of the HH model is the FHN model [8], [14]:  $dv/dt = a(-v(v-1)(v-b) - w + I)$ ,  $dw/dt = v - cw$ , where  $v$  is the membrane potential,  $w$  is the recovery variable,  $a$  and  $c$  are scaling parameters,  $I$  is a constant stimulus current, and all the variables are dimensionless.  $b$  (the spiking threshold) should be between zero and one, and to obtain electrical spiking, usually  $b < 0.5$  is chosen [22]. Consequently,  $b$  is an unstable equilibrium of  $dv/dt = a(-v(v-1)(v-b))$  and corresponds to the threshold between electrical silence and electrical spiking [2]. It is recommended to choose  $a \gg 1$  [12],  $c > 0$  and small enough [17]. For appropriate constant values of the parameters, it is possible to generate tonic spiking using FHN, i.e., the neuron spikes in a periodic manner.

Conventionally, the parameters in the FHN model are kept constant, and certain spiking behaviors such as bursting cannot be obtained using this model [11]. Since  $I$  is an external input, it can externally control the spiking mode observed in the output ( $v$ ), and induce spiking behaviors such as bursting [21]; on the other hand, the parameters  $a$ ,  $b$ , and  $c$  are governed by the mechanisms internal to the neuron, and their variations can be associated with some internal physiological system. We are interested in exploiting the possibility of time variations of these internal parameters leading to behaviors such as bursting because this method adds an internal spiking capability to the system. The justification of this approach is in the hypothesis that the time variations of these parameters are physiologically programmed within a neuron. This approach is different from [21] in the sense that variations in the parameters represent the changes in the mechanisms internal to the neuron versus the changes in the stimulus current and some external force. We consider variations in  $b$  because it is the threshold between electrical silence and neural spiking. Moreover, physiologically, it might be the case that this threshold is varying, causing the neurons to switch ON and OFF, and generate bursting. The spiking threshold might also be varying due to the stimulation. This phenomenon has been observed in several systems including the visual cortex, somatosensory cortex, prefrontal cortex, neostriatum, neocortex, hippocampus, and auditory brainstem using voltage-clamp experiments [15]. Moreover,  $b$  can control the spiking frequency. Hence, we propose that by varying  $b$  in the FHN model, it is possible to obtain spiking modes such as bursting and varying frequency spiking. Our proposed extension to the FHN model which includes a time-varying threshold is

$$\begin{aligned} \frac{dv}{dt} &= a(-v(v-1)(v-b) - w + I) \\ \frac{dw}{dt} &= v - cw, \quad \frac{db}{dt} = \varepsilon_b g(t) \end{aligned} \quad (1)$$

where  $b \equiv b(t)$ ,  $\varepsilon_b g(t)$  corresponds to the rate of change in the spiking threshold  $b$ , we assume  $\varepsilon_b \ll a$ , and  $g(t)$  can control the spiking frequency and also cause the neurons to switch ON and OFF. In this extension,  $\varepsilon_b \ll a$  suggests that the rate of change of the spiking threshold is much slower than the spiking activity. In other words,  $b(t)$  is a slowly varying function bounded between zero and one. The changes in  $b(t)$  are restricted to two kinds of functions. First is a class of functions in which the spiking threshold varies due to the stimulation. In this case, the spiking threshold  $b(t)$  can be modeled as concatenation of two (or more) functions where the spiking threshold varies due to the changes in the stimulus and then becomes constant. Second is a class of functions in which the periodic variations are programmed within the neuron. In this case, the spiking threshold  $b(t)$  can be modeled using a periodic function. An example of this is slow oscillations ( $< 1$  Hz), which occur periodically [19]. It is useful to note the differences between model (1) and the HR model. The HR model takes the form

$$\begin{aligned} \frac{dv}{dt} &= a(-v(v-1)(v-b) - w + n + I) \\ \frac{dw}{dt} &= v - cw, \quad \frac{dn}{dt} = 1 - sv^2 - n \end{aligned} \quad (2)$$

where  $n$  is another recovery variable, and  $s$  is a scaling parameter. Models (1) and (2) are different in the sense that the third differential equation in (2) depends on  $v$  while the third equation in (1) is not coupled to  $v$ . Also, the third differential equation in (1) describes the spiking threshold while the third differential equation in (2) describes a recovery variable. Hence, the proposed extension to the FHN model in (1) is simpler than the HR model in (2) and is still able to generate interesting spiking behaviors.

In the following sections, we demonstrate through illustrative examples that spiking patterns such as tonic bursting, mixed mode firing, neural spiking with nonincreasing frequency, and varying frequency neural spiking can be obtained using model (1). The simulations were performed using MATLAB/Simulink [13].

### A. Tonic Bursting

Tonic bursting is a spiking behavior in which a neuron fires a certain number of spikes in rapid succession and is then silent for a period of time. Then, it repeats this pattern in a periodic manner. For example, tonic bursting occurs in medullary preBötzinger complex of rats, which is essential to the respiratory activity [16]. We simulated model (1) for  $a = 10^5$ ,  $I = 1$ ,  $c = 0.2$ , and  $b(t) = 0.5 + 0.1 \sin(\frac{\pi}{6}t)$  with initial conditions  $(v, w) = (0, 0)$ . The resultant tonic bursting behavior is shown in Fig. 1. This is one possible way of varying  $b$  in order to obtain tonic bursting. Different sinusoidal functions or triangular waves could also be used.

### B. Mixed Mode Firing

Mixed mode is a spiking mode in which the neuron fires a single burst when the stimulus is applied and then switches to tonic spiking [11]. Some neurons such as lateral geniculate

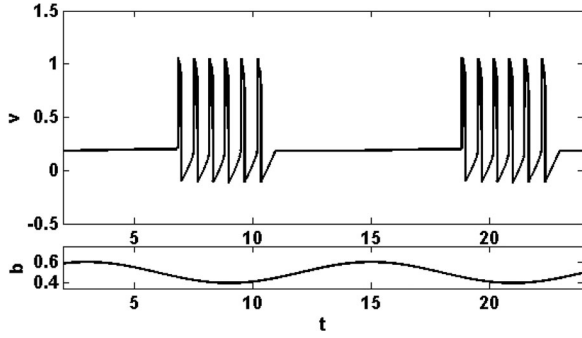


Fig. 1. Tonic bursting.

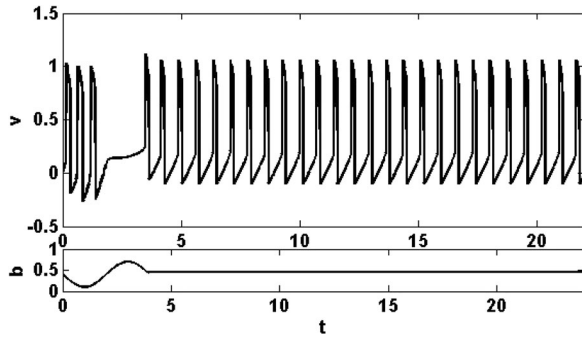


Fig. 2. Mixed mode firing.

nucleus neurons in the thalamus of ferrets exhibit mixed mode firing [4]. We generated a sample mixed mode firing behavior by simulating model (1) with initial conditions  $(v, w) = (0, 1)$  and parameters  $a = 10^5$ ,  $I = 1$ ,  $c = 0.2$ , and  $b(t)$  defined as follows:

$$b(t) = \begin{cases} 0.4 - 0.3 \sin(\frac{\pi}{2}t) & t < 3.9149 \\ 0.44 & 3.9149 \leq t < 24. \end{cases}$$

where this function could be repeated periodically. The resulting mixed mode firing pattern is shown in Fig. 2. This is one possible way of generating mixed mode. Another way is to use a triangular wave or a sinusoidal function at the beginning, and then keep the value of  $b$  constant.

### C. Neural Spiking With Nonincreasing Frequency

Neural spiking with nonincreasing frequency is another possible spiking mode obtained by varying  $b$ , in which the frequency of every spike is less than or equal to the frequency of the previous spike. Calcium oscillations in CHO-lac-mGlu5a cells of rats can exhibit such behavior under certain conditions [1]. We generated a sample mixed mode spiking behavior by simulating model (1) with initial conditions  $(v, w) = (0, 1)$ , and parameters  $a = 10^5$ ,  $I = 1$ ,  $c = 0.25$ , and  $b(t)$  defined as follows:

$$b(t) = \begin{cases} \frac{1}{10}t & t < 5.5 \\ 0.55 & 5.5 \leq t < 24. \end{cases}$$

The resulting spiking mode with nonincreasing frequency is shown in Fig. 3.

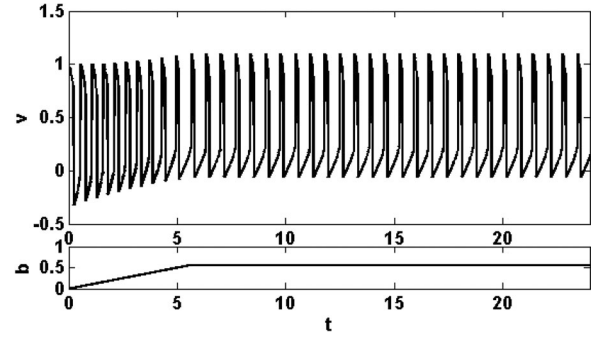


Fig. 3. Neural spiking with nonincreasing frequency.

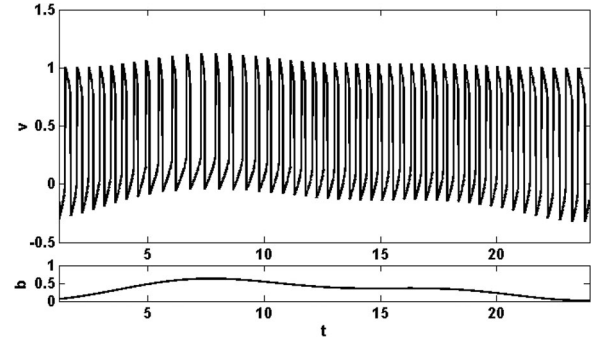


Fig. 4. Varying frequency neural spiking.

### D. Varying Frequency Neural Spiking

Finally, we illustrate that neural spiking with varying frequency can be obtained using model (1). In this spiking activity, the frequency of every spike varies compared to the frequency of the previous spike. Neural spiking with varying frequency occurs, for example, in the respiratory center of the mouse [9]. We generated a varying frequency neural spiking behavior by simulating model (1) for  $a = 10^5$ ,  $I = 1$ ,  $c = 0.3$ , and  $b(t) = \frac{1}{30}(10 - 6 \cos(\frac{2\pi t}{24}) + 3.5 \sin(\frac{2\pi t}{24}) - 3.5 \cos(\frac{4\pi t}{24}) - 1.1720 \sin(\frac{4\pi t}{24}))$  with initial conditions  $(v, w) = (0, 0)$ . The resulting varying frequency neural spiking mode is shown in Fig. 4. It is also possible to use other two harmonic functions for  $b(t)$  to obtain similar spiking patterns.

The examples in Sections II-A–II-D suggest that by varying the spiking threshold using a time-varying function  $b(t)$ , one could obtain a richer set of spiking behaviors than possible by the classical FHN model with fixed spiking threshold. Although some of the examples presented use discontinuous  $g(t)$ , a smooth approximation of  $g(t)$  will have the same effect in obtaining the desired spiking activity.

## III. PARAMETER ESTIMATION

The parameter estimation for the HH, HR, and FHN models is usually done using model-free methods such as simulated annealing, genetic algorithms, differential evolution [3], EKF, or adaptive observers [7], [20], [23]. For the class of HR and FHN models, using coordinate transformation, it is possible to represent the system in the adaptive observer canonical form and develop an observer to estimate the parameters of the neuron

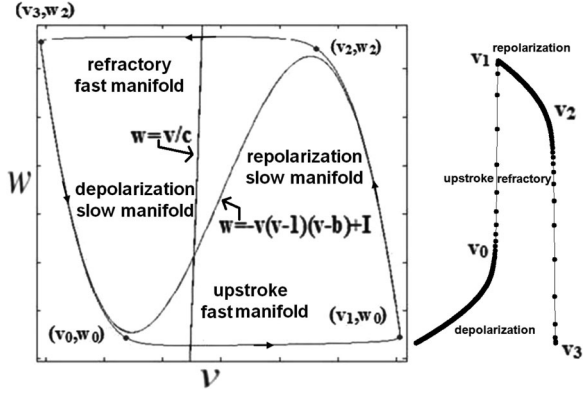


Fig. 5. (Left) Phase portrait and (right) time series plot of the FHN model during a tonic spiking mode. The dots show how one spike looks when a sampling interval of  $10^{-3}$  for the dimensionless system (for the case of a spiking neuron, the units are in milliseconds, i.e., a sampling interval of  $10^{-3}$  ms) is used for simulating tonic spiking.

with an exponential convergence rate [7], [23]. In principle, if the model has a known structure, one could exploit it to formulate a parameter estimation method customized to that model and tune it to get better performance than model-free methods that do not take advantage of the structure of the model. In the following, we develop one such method, which we refer to as the FSD estimation algorithm, for estimating the parameter  $b$  for the FHN model by exploiting the fast-slow dynamics of FHN. We then compare the performance of FSD and EKF and show that FSD outperforms EKF in several scenarios. The potential of the FHN model to lend itself to an efficient estimation method such as FSD further reinforces the utility of the FHN model, this time from the estimation point of view.

#### A. Estimation Algorithm for Constant Spiking Threshold in the FHN Model

In this section, we first summarize the behavior of the FHN model in the phase plane. Based on this, we then develop a set of constraints that the spiking threshold  $b$  has to satisfy. These constraints motivate the cost function used in FSD estimation algorithm.

When the FHN model is in tonic spiking mode, the system goes through a limit cycle in the phase plane. Fig. 5 shows the phase portrait and corresponding time series plot of the FHN model during a typical tonic spiking mode. The phase portrait shows that, in the case of tonic spiking mode, the trajectories switch between *slow scale dynamics* (that correspond to depolarization/repolarization) and *fast scale dynamics* (that correspond to upstroke/refractory). We develop a novel algorithm that exploits this two-time-scale feature of the FHN model to provide accurate estimates of the spiking threshold  $b$  with the time series plot of membrane potentials  $v$  as input.

We now derive constraints imposed on  $b$  by a given time series data of  $v$ . The procedure described in the following is inspired by the limiting behavior of the trajectories of the FHN model in the phase plane for  $a \gg 1$ . In particular, for such a limiting case, since  $v$  does not change significantly when the model is following the slow time-scale dynamics, we approx-

imate its derivative to be zero over the slow time-scale dynamics. If  $dv/dt = 0$ , then  $w = -v(v-1)(v-b) + I$ . Then, define  $f$  as  $f(v, b, I) := -v(v-1)(v-b) + I$ , where  $f$  corresponds to the cubic nullcline of the FHN model. Let  $v_2$  and  $v_0$  be the values of  $v$  that maximize and minimize  $f$ , respectively:  $v_0 = \frac{1}{3}(b+1 - \sqrt{b^2 - b + 1})$ ,  $v_2 = \frac{1}{3}(b+1 + \sqrt{b^2 - b + 1})$ .

Let  $w_2$  and  $w_0$  be the values of  $w$  corresponding to  $v_2$  and  $v_0$ , respectively, in the phase plane. As observed in Fig. 5,  $w_2$  and  $w_0$  do not exactly correspond to the maximum and minimum values of  $f$ ; however, we can approximate  $w_2$  and  $w_0$  by plugging in the values of  $v_2$  and  $v_0$  in  $f(v, b, I)$ . The resulting values of  $w_0$  and  $w_2$  are given by

$$w_0 \approx -\frac{2}{27}\sqrt{(b^2 - b + 1)^3} + \frac{2}{27}b^3 - \frac{1}{9}b^2 - \frac{1}{9}b + \frac{2}{27} + I$$

$$w_2 \approx \frac{2}{27}\sqrt{(b^2 - b + 1)^3} + \frac{2}{27}b^3 - \frac{1}{9}b^2 - \frac{1}{9}b + \frac{2}{27} + I.$$

Let  $h_0(b) := w_0 - I$  and  $h_2(b) := w_2 - I$ . Then

$$h_0(b) - h_2(b) = -\frac{4}{27}\sqrt{(b^2 - b + 1)^3} \quad (3)$$

$$h_0(b) + h_2(b) = \frac{4}{27}b^3 - \frac{2}{9}b^2 - \frac{2}{9}b + \frac{4}{27}. \quad (4)$$

From the  $v$  time series data, it is possible to obtain the maximum and minimum values of  $v$ ,  $v_1$ , and  $v_3$ , respectively. As observed in Fig. 5, the  $w$  values that, respectively, correspond to  $v_1$  and  $v_3$  in the phase plane satisfy the cubic nullcline equation and are approximately equal to  $w_0$  and  $w_2$ , respectively (because  $dw/dt \approx 0$  on the fast manifolds). Hence, the following system of equations is obtained

$$f(v_1, b, I) \approx w_0 \Rightarrow -v_1(v_1 - 1)(v_1 - b) \approx h_0(b)$$

$$f(v_3, b, I) \approx w_2 \Rightarrow -v_3(v_3 - 1)(v_3 - b) \approx h_2(b).$$

This system of equations can be simplified using (3) and (4) as

$$\begin{aligned} & -v_1(v_1 - 1)(v_1 - b) + v_3(v_3 - 1)(v_3 - b) \\ & \approx h_0(b) - h_2(b) = -\frac{4}{27}\sqrt{(b^2 - b + 1)^3} \end{aligned} \quad (5)$$

$$\begin{aligned} & -v_1(v_1 - 1)(v_1 - b) - v_3(v_3 - 1)(v_3 - b) \\ & \approx h_0(b) + h_2(b) = \frac{4}{27}b^3 - \frac{2}{9}b^2 - \frac{2}{9}b + \frac{4}{27}. \end{aligned} \quad (6)$$

Equations (5) and (6) may not admit a common solution  $b$ . Therefore, we look for the  $b$  that minimizes the sum of absolute errors in satisfying the two equations.

Based on the aforementioned analysis, we propose the following algorithm for estimating the spiking threshold  $b$  when the system is in the spiking mode. The second and third steps of the algorithm correspond to finding the equality cost function for (5) and (6).

#### Fast-Slow Dynamics Estimation Algorithm

- 1) Obtain the maximum and minimum values of  $v$  time series, and denote them by  $v_1$  and  $v_3$ , respectively.
- 2) Let  $y(b) := -v_1(v_1 - 1)(v_1 - b) + v_3(v_3 - 1)(v_3 - b) + \frac{4}{27}\sqrt{(b^2 - b + 1)^3}$ , and  $z(b) := -v_1(v_1 - 1)(v_1 - b) - v_3(v_3 - 1)(v_3 - b) - \frac{4}{27}b^3 + \frac{2}{9}b^2 + \frac{2}{9}b - \frac{4}{27}$ .

TABLE I  
ESTIMATES OF  $b$  USING THE FSD METHOD

$b$	$b_{estimate}$	percent error
0.05	0.0499	0.20
0.10	0.0998	0.20
0.15	0.1497	0.20
0.2	0.1996	0.20
0.25	0.2495	0.20
0.3	0.2993	0.23
0.35	0.3493	0.20
0.4	0.3991	0.22
0.45	0.4490	0.22
0.5	0.4989	0.22
0.55	0.5488	0.22
0.6	0.5986	0.23
0.65	0.6485	0.23
0.7	0.6984	0.23

- 3) The  $b$  estimate corresponds to the solution of the following optimization problem

$$\operatorname{argmin}_{b \in [0,1]} |y(b)| + |z(b)|.$$

We implemented the FSD algorithm on simulated time series data as follows. The values of  $a$ ,  $I$ , and  $c$  were fixed at  $10^5$ , 1, and 0.3, respectively. The values of  $b$  were chosen to be from 0.05 to 0.7 (above which there is no tonic spiking) in increments of 0.05. For each value of  $b$ , a time series of membrane potentials  $v$  is generated by simulating the FHN model and the FSD algorithm is implemented on this time series data to get an estimate of  $b$ . The estimated values of  $b$  as well as the percent error are shown in Table I. As observed in Table I, the error is uniformly less than 0.3%.

### B. Comparison of FSD and EKF Performance for Tonic Spiking

In the previous section, a novel approach for estimating  $b$  was proposed. In this section, we compare the  $b$  estimates given by FSD and EKF. In order to compare FSD with EKF, process noise and sensor noise were incorporated into the simulations according to the following model:

$$\begin{aligned} dv &= a(-v(t)(v(t) - 1)(v(t) - b) - w(t) + I)dt + \sigma_p d\eta \\ dw &= (v(t) - cw(t))dt + \sigma_p d\eta, \quad db = \sigma_p d\eta \\ v_{\text{obs}} &= v + \sigma_s \zeta \end{aligned} \quad (7)$$

where  $\sigma_p$  and  $\sigma_s$  represent the standard deviation in the process noise and the sensor noise, respectively.  $\eta$  and  $\zeta$  represent the Wiener process and a standard normal random variable, respectively, and  $v_{\text{obs}}$  is the observed membrane potential. Several time series for membrane potentials  $v_{\text{obs}}$  were generated by simulating (7) with parameters fixed across all the time series being  $a = 10^5$ ,  $I = 1$ ,  $c = 0.3$ ,  $b = 0.5$ , and  $\sigma_p = 0.1$ , while different values of  $\sigma_s$  were chosen for different time series as described in the following examples. In order to implement FSD on a time series data, 24 tonic spikes were averaged to give data points for a single spike, which was then used as an input to FSD. In order to implement EKF, we discretized (7) using forward Euler method with a sampling interval  $\Delta$ , where  $\Delta$  was again varied across different time series as described in the following examples. In each example, the same sampling interval was

used for generating the data for implementing FSD. For EKF implementation, actual initial condition values were chosen to be the initial estimates, and the initial covariance estimate was set to zero.

- 1) In this example,  $\sigma_s = 0.001$  was chosen to generate time series of  $v_{\text{obs}}$ . The  $b$  estimate obtained from FSD was 0.4980, which corresponds to 0.4% error. EKF was implemented with  $\Delta = 10^{-5}$ , and the  $b$  estimate after processing data equivalent to one tonic spike was 0.5001, which corresponds to 0.02% error. In this example, the sampling rate for EKF was very high and the sensor noise was very low, putting EKF in an advantage.
- 2) In this example,  $\sigma_s = 0.01$  and  $\Delta = 10^{-5}$  were used. The  $b$  estimate obtained by FSD was 0.4932, which corresponds to 1.3559% error. The  $b$  estimates from EKF, on the other hand, did not converge and varied between 0.1358 and 1.47.
- 3) In this example,  $\sigma_s = 0.001$  and  $\Delta = 10^{-3}$  were used. The  $b$  estimate obtained by FSD was 0.4929, which corresponds to 1.4199% error. The  $b$  estimates from EKF, on the other hand, diverged.

Hence, comparing the two methods, EKF is more sensitive to the sampling interval  $\Delta$  than FSD. FSD is less affected by the sampling interval because FSD only requires the knowledge of the maximum and minimum values of  $v_{\text{obs}}$  for its implementation, and when we increase the sampling interval, the maximum and minimum values obtained are close to the actual ones. Moreover, EKF does not converge if the sensor noise variance is large.

### C. Estimation Algorithm for Time-Varying Spiking Threshold in the FHN Model

In this section, using examples, we illustrate that the FSD estimation algorithm for constant  $b$  can also be employed for neural spiking data generated by time-varying  $b$ , provided one has knowledge about the structure of the time variations of  $b$ , e.g., impulsive, harmonic, etc. The time series data were generated by simulating the FHN model with time-varying  $b$  and by adding sensor and process noise. In order to implement FSD for a specific time-varying  $b$ , we averaged all the corresponding time series data to obtain a *mean* time series data. For this mean time series data, we obtained the membrane potential peaks, and broke the data into segments corresponding to peak-to-peak intervals. Then, using FSD algorithm for estimating constant  $b$  as developed in Section III-A, we estimated  $b$  for each of these segments, and associated each of these estimates with the corresponding time segment. This gives a time series of  $b$  estimates. Then, utilizing the knowledge of the structure of  $b$ , we implemented multiple or linear regression (depending on the structure of  $b$ ) to fit a function to the  $b$  estimate time series. In the cases that  $b$  was known to be concatenation of two (or more) different functions, we broke the data into two (or more) parts at the point(s) that the functions were concatenated, and depending on the function in each part, linear or multiple regression was used to fit the  $b$  estimates in each part.

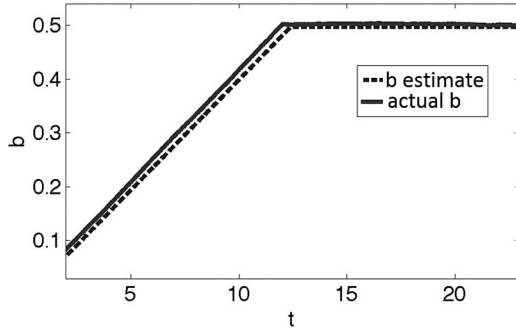


Fig. 6. Parameter estimation for neural spiking with nonincreasing frequency using the FSD algorithm.

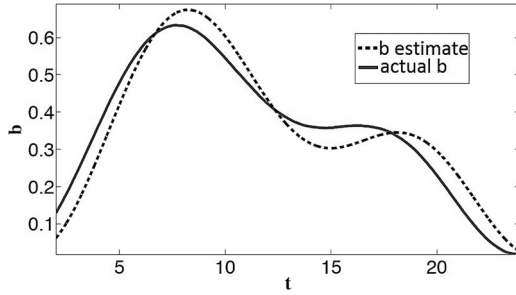


Fig. 7. Parameter estimation for varying frequency neural spiking using the FSD algorithm.

Figs. 6 and 7 illustrate the results obtained from implementation of the FSD algorithm on neural spiking with nonincreasing frequency and time-varying frequency neural spiking data. Fig. 6 shows the plot of  $b(t)$  for neural spiking with nonincreasing frequency, as defined in (8) and its estimate using the FSD algorithm

$$b(t) = \begin{cases} \alpha t + \beta & t < t_0 \\ \alpha t_0 + \beta & t_0 \leq t < 24. \end{cases} \quad (8)$$

Fig. 7 shows the plot of  $b(t)$  for time-varying frequency neural spiking, as defined in (9) and its estimate using the FSD algorithm

$$b(t) = \alpha + \beta \cos\left(\frac{2\pi t}{24}\right) + \gamma \sin\left(\frac{2\pi t}{24}\right) + \zeta \cos\left(\frac{2\pi t}{12}\right) + \kappa \sin\left(\frac{2\pi t}{12}\right). \quad (9)$$

In the next section, we report the results from the comparison of FSD and EKF on the data corresponding to tonic bursting.

#### D. Comparison of FSD and EKF Performance for Tonic Bursting

In this section, we compare the FSD algorithm with EKF for tonic bursting, which can be obtained using a sinusoidal  $b$ . For this comparison, process noise and sensor noise were incorporated into the simulations according to the following model:

$$dv = (a(-v(v-1)(v - (\alpha \sin(\lambda t + \beta) + \gamma)) - w + I))dt$$

TABLE II  
COMPARISON OF PARAMETER ESTIMATES OBTAINED BY FSD AND EKF FOR EXAMPLE 1 FOR TIME-VARYING  $b$

	FSD estimate	FSD error	EKF's estimate	EKF's error
$\alpha=0.5$	0.5053	1.068%	0.5	0%
$T=12$	11.933	0.5583%	12	0%
$\cos(\beta)=1$	0.9999	0.010%	1	0%
$\gamma=0.5$	0.5006	0.1207%	0.5	0%

$$\begin{aligned} & + \sigma_p d\eta \\ dw &= (v - cw)dt + \sigma_p d\eta, \quad d\gamma = \sigma_p d\eta \\ d\alpha &= \sigma_p d\eta, \quad d\lambda = \sigma_p d\eta \\ d\beta &= \sigma_p d\eta, \quad v_{\text{obs}} = v + \sigma_s \zeta \end{aligned} \quad (10)$$

where  $\sigma_p$  and  $\sigma_s$  represent the standard deviation in the process noise and the sensor noise, respectively.  $\eta$  and  $\zeta$  represent the Wiener process and a standard normal random variable, respectively, and  $v_{\text{obs}}$  is the observed membrane potential. Five  $v_{\text{obs}}$  time series were generated by simulating (10) with the parameters fixed across all the time series being  $a = 10^5$ ,  $I = 1$ ,  $c = 0.3$ , and  $\sigma_p = 0.1$ , while different values of  $\sigma_s$  were chosen for different time series as described in the following examples. We obtained the time series of  $b$  estimates from neural spiking time series data using FSD in the same way as in Section III-C. Then, knowing that  $b$  is a sinusoid of the form  $\alpha \sin(\frac{2\pi}{T}t + \beta) + \gamma$ , we estimated the period  $T$  from the time series plot of  $b$  estimates by inspection. Finally, using the trigonometric identity  $\alpha \sin(\frac{2\pi}{T}t + \beta) + \gamma = \alpha \sin(\frac{2\pi}{T}t) \cos(\beta) + \alpha \cos(\frac{2\pi}{T}t) \sin(\beta) + \gamma$ , we implemented multiple regression to find the coefficients  $\alpha$ ,  $\beta$ , and  $\gamma$ . In order to implement EKF, we discretized (10) using forward Euler method with a sampling interval  $\Delta$ , where  $\Delta$  was again varied across different time series as described in the following examples. In each example, the same sampling interval was used for generating the data for implementing FSD. For the EKF implementation, actual initial condition values were chosen to be the initial estimates, and the initial covariance estimate was set to zero.

- 1) In this example,  $\sigma_s = 0.001$  and  $\Delta = 10^{-5}$  were chosen to generate the time series of  $v_{\text{obs}}$ . We implemented FSD and EKF, and obtained the parameter estimates and the corresponding percent error for each of the parameters, which are reported in Table II. In reporting the EKF estimates, we ignored the estimates for which the entries of the error covariance matrix became very large. The EKF algorithm outperforms FSD when the process noise is low and the sampling rate is high.
- 2) In this example,  $\sigma_s = \sqrt{0.1}$  and  $\Delta = 10^{-5}$  were used to implement FSD and EKF. The EKF parameter estimates became very noisy; however, the average value of the noisy parameter estimates obtained by EKF had a small error, and, here, we are reporting the average value of the noisy estimates as the EKF parameter estimate. The parameter estimates and the corresponding percent error for each of the parameters are reported in Table III.

TABLE III  
COMPARISON OF PARAMETER ESTIMATES OBTAINED BY FSD AND EKF FOR  
EXAMPLE 2 FOR TIME-VARYING  $b$

	FSD estimate	FSD error	EKF's estimate	EKF's error
$\alpha=0.5$	0.4978	0.4367%	0.5045	0.9%
$T=12$	11.933	0.5583%	12.1461	1.2176%
$\cos(\beta)=1$	0.999	0.1%	1	0%
$\gamma=0.5$	0.4982	0.3600%	0.5062	1.24%

TABLE IV  
COMPARISON OF PARAMETER ESTIMATES OBTAINED BY FSD AND EKF FOR  
EXAMPLE 3 FOR TIME-VARYING  $b$

	FSD estimate	FSD error	EKF's estimate	EKF's error
$\alpha=0.5$	0.4897	2.0545%	Diverged	NA
$T=12$	12.029	0.2417%	Diverged	NA
$\cos(\beta)=1$	1	0%	Diverged	NA
$\gamma=0.5$	0.4944	1.1115%	Diverged	NA

3) In this example,  $\sigma_s = 0.001$  and  $\Delta = 10^{-3}$  were used and parameter estimates reported in Table IV were obtained using FSD, while EKF diverged.

Through three examples, we showed how one could implement the FSD method for the case that  $b$  is a time-varying function. Then, comparing this algorithm with EKF, we showed that FSD performed better than EKF when the sampling rate was low.

#### IV. CONCLUSION, DISCUSSION, AND FUTURE WORK

The proposed approach in extending the FHN model by varying its parameters allows for simulating more complex behaviors than the ones that are possible by keeping the parameters constant. In this paper, variations in the threshold between electrical silence and electrical spiking were investigated. Then, an estimation algorithm (the FSD algorithm) that exploits the fast-slow dynamics of FHN was proposed. For constant  $b$ , the proposed algorithm performed better than EKF when the sampling interval was high or when the sensor noise variance was high. For time-varying  $b$ , the FSD estimation algorithm performed better than EKF when the sampling interval was high. Another advantage of the FSD algorithm over EKF is that when  $b$  is time varying, and the structure of  $b(t)$  is unknown, time series of  $b$  estimates can be obtained using FSD, which could add insight into the structure of  $b(t)$ . For the cases that  $b(t)$  is reasonably slow, EKF can be implemented on one spike repeatedly until it converges, while neglecting the other spikes that are generated in the meantime. Once convergence is achieved for this spike, EKF can be implemented on the spike generated at that moment. One can repeat this process to obtain  $b$  estimates for the case that the structure of  $b$  is unknown. Using this approach, EKF neglects the spikes generated in between convergence, while FSD gives a  $b$  estimate for every spike in the spike train. Hence, FSD performs better than EKF in understanding the structure of the spiking threshold. However, if the goal is not to perform online estimation, EKF can be implemented on one spike repeatedly until it converges, and this process can be repeated on all the spikes in the spike train. Using this approach, for every spike in the spike train, a  $b$  estimate can be obtained, which adds insight in understanding the structure of  $b(t)$ . Hence, FSD and

EKF can both be used to understand the structure of the spiking threshold when online estimation is not a concern. Moreover, in order to run EKF in the discussed examples, it was assumed that the values of  $a$ ,  $I$ , and  $c$  are known while FSD does not require knowledge of the parameters  $a$ ,  $I$ , and  $c$ , and estimates  $b$  only based on  $v$  time series data. The proposed method for estimating the spiking threshold is limited to the structure of the FHN model. Moreover, the estimation results presented are for the case that  $a$  is very large, which results in fast dynamics, as typically observed in physiological data. This is in contrast with model-free methods such as EKF or adaptive observers whose implementation is not restricted by the structure of the model.

In our future work, we plan to extend our model and estimation method to other parameters of the FHN model. We also plan to explore the physiological factors determining the parameter variations that lead to variations in neural spiking patterns and implement the FSD estimation algorithm on physiological data.

#### REFERENCES

- [1] S. J. Bradley, J. M. Watson, and R. A. J. Challiss, "Effects of positive allosteric modulators on single cell oscillatory  $\text{Ca}^{2+}$  signaling initiated by the type 5 metabotropic glutamate receptor," *Amer. Pharmacol. Exp. Therapeut.*, vol. 76, pp. 1302–1313, 2009.
- [2] D. Brown, A. E. Herbison, J. E. Robinson, R. W. Marrs, and G. Leng, "Modeling the luteinizing hormone-releasing hormone pulse generator," *J. Neuroendocrinol.*, vol. 63, no. 3, pp. 869–879, 1994.
- [3] L. Buhry, A. Saighi, E. Giremus, and S. Renaud, "Parameter estimation of the Hodgkin–Huxley model using metaheuristics: Applications to neuromimetic analog integrated circuits," in *Proc. IEEE Biomed. Circuits Syst. Conf.*, 2008, pp. 173–176.
- [4] M. Esguerra and M. Sur, "Spike trains and signaling modes of neurons in the ferret lateral geniculate nucleus," *Exp. Brain Res.*, vol. 96, pp. 273–286, 1993.
- [5] R. T. Faghih, K. Savla, M. Dahleh, and E. N. Brown, "The FitzHugh–Nagumo model: Firing modes with time varying parameters and parameter estimation," in *Proc. Annu. Int. Conf. IEEE Eng. Med. Biol. Soc.*, Buenos Aires, Argentina, 2010, pp. 4116–4119.
- [6] R. T. Faghih, "The FitzHugh–Nagumo model dynamics with an application to the hypothalamic pituitary adrenal axis," M.S. thesis, Dept. Elect. Eng. Comput. Sci., Massachusetts Inst. Technol., Cambridge, 2010.
- [7] D. Fairhurst, I. Yu. Tyukin, H. Nijmeijer, and C. van Leeuwe, "Observers for canonic models of neural oscillators," *Math. Model. Natural Phenomena*, vol. 5, no. 2, pp. 146–184, 2010.
- [8] R. FitzHugh, "Impulses and physiological states in theoretical models of nerve membrane," *Biophys. J.*, vol. 1, no. 6, pp. 445–466, 1961.
- [9] F. Han, S. Subramanian, E. R. Price, J. Nadeau, and K. P. Strohl, "Periodic breathing in the mouse," *J. Appl. Physiol.*, vol. 92, no. 3, pp. 1133–1140, 2002.
- [10] A. L. Hodgkin and A. F. Huxley, "A quantitative description of membrane current and its application to conduction and excitation in nerve," *J. Physiol.*, vol. 117, no. 4, pp. 500–544, 1952.
- [11] E. M. Izhikevich, "Which model to use for cortical spiking neurons?," *IEEE Trans. Neural Netw. (Spec. Issue Temporal Cod.)*, vol. 15, no. 5, pp. 1063–1070, Sep. 2004.
- [12] A. Labbi, R. Milanese, and H. Bosch, "Gray-level object segmentation with a network of FitzHugh–Nagumo oscillators," in *Proc. Biol. Artif. Comput.: Neurosci. Technol.*, Berlin, Germany, 1997, vol. 1240, pp. 1075–1084.
- [13] MATLAB R2009a, MathWorks Inc., Natick, MA, 2009.
- [14] J. Nagumo, S. Arimoto, and S. Yoshizawa, "An active pulse transmission line simulating nerve axon," *Proc. Inst. Radio Eng.*, vol. 50, no. 10, pp. 2061–2070, 1962.
- [15] J. Platkiewicz and R. Brette, "Impact of fast sodium channel inactivation on spike threshold dynamics and synaptic integration," *PLoS Comput. Biol.*, vol. 7, no. 5, e1101129, p. 15, 2011.
- [16] A. R. Radulescu, "Respiratory rhythm generation during gasping depends on persistent sodium current," *Nature Neurosci.*, vol. 9, pp. 311–313, 2006.

- [17] J. Rinzel and J. P. Keener, "Hopf bifurcation to repetitive activity in nerve," *SIAM J. Appl. Math.*, vol. 43, no. 4, pp. 907–922, 1983.
- [18] R. M. Rose and J. L. Hindmarsh, "The assembly of ionic currents in a thalamic neuron I. The three-dimensional model," *Proc. Roy. Soc. B: Biol. Sci.*, vol. 237, no. 1288, pp. 267–288, 1989.
- [19] M. Steriade, A. Nunez, and F. Amzica, "A novel slow (< 1 Hz) oscillation of neocortical neurons in vivo: Depolarizing and hyperpolarizing components," *J. Neurosci.*, vol. 13, no. 8, pp. 3252–3265, Aug. 1, 1993.
- [20] I. Tokuda, U. Parlitz, L. Illing, M. Kennel, and H. Abarbanel, "Parameter estimation for neuron models," in *Proc. 7th Exp. Chaos Conf.*, San Diego, CA, 2002, vol. 676, pp. 251–256.
- [21] S. Tsuji, T. Ueta, H. Kawakami, and K. Aihara, "An advanced design method of bursting in FitzHugh–Nagumo model," in *Proc. IEEE Int. Symp. Circuits Syst.*, 2002, vol. 1, pp. 1-389–1-392.
- [22] H. C. I. Tuckwell, R. Rodriguez, and F. Y. M. Wan, "Determination of firing times for the stochastic FitzHugh–Nagumo neuronal model," *Neural Comput.*, vol. 15, no. 1, pp. 143–159, 2003.
- [23] I. Tyukin, E. Steur, H. Nijmeijer, D. Fairhurst, I. Song, A. Semyanov, and C. van Leeuwen, "State and parameter estimation for canonic models of neural oscillators," *Int. J. Neural Syst.*, vol. 20, no. 3, pp. 193–207, 2010.



**Rose T. Faghih** (S'12) received the B.S. degree (*summa cum laude*) in electrical engineering (Hons.) from the University of Maryland, College Park, and the S.M. degree in electrical engineering and computer science from the Massachusetts Institute of Technology (MIT), Cambridge, in 2008 and 2010, respectively. She is currently a Ph.D. candidate in the Department of Electrical Engineering and Computer Science, MIT, where she is affiliated with the Laboratory for Information and Decision Systems, and the Neuroscience Statistics Research Laboratory.

Prior to joining MIT, she participated in the National Science Foundation Research Experiences for Undergraduates Programs at Drexel University in the summer of 2006 and at the University of Maryland in the summer of 2007. Her research interests include estimation, modeling, and control of endocrine and neural systems, and computational neuroscience.

Ms. Faghih is a National Science Foundation Graduate Fellow, and the recipient of an MIT Graduate Fellowship. She received various scholarships and awards during her undergraduate studies, including the University of Maryland Presidential Scholarship, the Society of Women Engineers Scholarship, and the Department of Electrical and Computer Engineering Chair's Award. She was also inducted into various honor societies including Phi Kappa Phi, Tau Beta Pi, Eta Kappa Nu, Golden Key International, and Primannum Honor Society.



**Ketan Savla** received the B.Tech. degree in mechanical engineering from the Indian Institute of Technology Bombay, Mumbai, India, in 2003, the M.S. degree in mechanical engineering from the University of Illinois at Urbana–Champaign, Urbana, in 2004, and the M.A. degree in applied mathematics and the Ph.D. degree in electrical engineering from the University of California at Santa Barbara (UCSB), Santa Barbara, both in 2007.

He is currently a Research Scientist in the Laboratory for Information and Decision Systems, Massachusetts Institute of Technology, Cambridge. His current research interests include control and optimization techniques for mobile autonomous systems, human-in-loop systems, complex service networks, and computational neuroscience.

Dr. Savla was awarded the 2005 Conference on Decision and Control and European Control Conference Best Student Paper Finalist and the Center for Control, Dynamical Systems, and Computation best thesis from UCSB.



**Munther A. Dahleh** (S'84–M'87–SM'97–F'01) was born in 1962. He received the B.S. degree in electrical engineering from Texas A&M University, College Station, and the Ph.D. degree in electrical engineering from Rice University, Houston, TX, in 1983 and 1987, respectively.

Since then, he has been with the Department of Electrical Engineering and Computer Science, MIT, Cambridge, where he is currently a Full Professor and the Associate Head. He is the coauthor (with I. Diaz-Bobillo) of the book *Control of Uncertain Sys-*

*tems: A Linear Programming Approach* (Englewood Cliffs, NJ: Prentice-Hall, 1995) and the coauthor (with N. Elia) of the book *Computational Methods for Controller Design* (New York: Springer, 1998). His research interests include problems at the interface of robust control, filtering, information theory, and computation. In addition to methodology development, he has been interested in the application of distributed control in the future electric grid and the future transportation system. He is also interested in various problems in network science. He is also interested in the interface between systems theory and neurobiology, and, in particular, in providing an anatomically consistent model of the motor control.

Dr. Dahleh served as an Associate Editor of the IEEE TRANSACTIONS ON AUTOMATIC CONTROL and of *Systems and Control Letters*. He has been the recipient of the Ralph Budd Award in 1987 for the best thesis at Rice University, the George Axelby Outstanding Paper Award (paper coauthored with J. B. Pearson in 1987), the National Science Foundation Presidential Young Investigator Award in 1991, the Finmeccanica Career Development Chair in 1992, the Donald P. Eckman Award from the American Control Council in 1993, the Graduate Students Council Teaching Award in 1995, the George Axelby Outstanding Paper Award (paper coauthored with Bamieh and Paganini in 2004), and the Hugo Schuck Award for Theory (for the paper coauthored with Martins). He was a Plenary Speaker at the 1994 American Control Conference, at the Mediterranean Conference on Control and Automation in 2003, at the Mathematical Theory for Networks and Systems in 2006, at the Symposium on System Identification in 2009, at Asian Control Conference in 2009, and at the Sixth Spanish, Italian, and Netherlands Meeting on Game Theory in 2010.



**Emery N. Brown** (M'01–SM'06–F'08) received the B.A. degree from Harvard College, Cambridge, MA, the M.D. degree from Harvard Medical School, Boston, MA, and the A.M. and Ph.D. degrees in statistics from Harvard University, Cambridge.

He is currently a Professor of computational neuroscience and health sciences and technology in the Department of Brain and Cognitive Sciences, Harvard–Massachusetts Division of Health Sciences and Technology, Massachusetts Institute of Technology, Cambridge, the Warren M. Zapol Professor of anesthesia at Harvard Medical School, and an Anesthesiologist in the Department of Anesthesia, Critical Care and Pain Medicine, Massachusetts General Hospital, Cambridge. His research interests include signal processing algorithms for the study of neural systems, functional neuroimaging, and electrophysiological approaches to study general anesthesia in humans.

Dr. Brown is a member of the Association of University Anesthesiologists. He is also a Fellow of the American Statistical Association, a Fellow of the American Association for the Advancement of Science, and a member of the Institute of Medicine. He was the recipient of the 2007 National Institutes of Health Directors Pioneer Award and the 2011 National Institute of Statistical Sciences Sacks Award for Outstanding Cross-Disciplinary Research. He was a Plenary Speaker at the IEEE International Symposium on Information Theory in 2007, and at the Annual International Conference of the IEEE Engineering in Medicine and Biology Society in 2010.